Laguerre-SVD Reduced-Order Modeling of a Yee-Cell-Based Discretisation of Maxwell's Equations

G. Lippens, D. De Zutter, F. Olyslager

Dept. of Information Technology (INTEC), Ghent University, Sint-Pietersnieuwstraat 41, B-9000 Gent, Belgium

Received 26 September 2003; accepted 7 August 2004

ABSTRACT: This article introduces a new method which combines a Yee-cell-based discretisation of Maxwell's equations and reduced-order modeling (ROM). The specific approach presented here handles both high-frequency and low-frequency parts of the simulation bandwidth. The combination of the robust Laguerre-SVD (LSVD) method and a Laplace-transformed state-space description of the discretised Maxwell's equations makes this broadband robustness possible. Three interconnection-type problems illustrate the feasibility of the new approach. © 2005 Wiley Periodicals, Inc. Int J RF and Microwave CAE 15: 187–196, 2005.

Keywords: Maxwell; state-space description; reduced-order modeling; Laguerre-SVD; iterative technique

I. INTRODUCTION

There is a clear demand for simulation tools that incorporate the full-wave behavior of passive interconnects and at the same time provide the designer with a lumped-circuit representation or a pole/zero model for further use in overall system simulations and optimisation. The well-known quasi-static approximations, such as in PEEC-based methods [1], suffer the inconvenience that the accuracy at the upper part of the spectrum decreases. A well-known method that does incorporate full-wave behavior is the finite-difference time-domain (FDTD) method. There are two drawbacks to be considered though. In order to correctly model the geometrical details of typical interconnection structures, rather small Yee cells are required. The Courant limit [2] then imposes a very small time step and hence very long CPU-times are needed. A second disadvantage for the designer is the postprocessing of the time signals that is necessary in order to obtain a frequency-domain transfer function from which a lumped-element network or a pole/zero model can be constructed, in particular when passivity must remain guaranteed. More powerful techniques capable of handling complex geometries and a large number of unknowns have been developed in recent years. We would in particular like to mention the finite-integration technique (FIT) [3] and the MAFIA [4] code built on this technique. In this article, we will restrict ourselves to a space discretisation using traditional Yee cells, but attention will be focused on the advantages offered by the application of a specific reduced-order modeling [5, 6] technique, the Laguerre-SVD algorithm [7, 8].

The combination of the Yee-cell-based discretisation of Maxwell's equations and reduced-order modeling is a recent research topic [9–13]. Before discussing the theoretical framework, we would like to remark that a combination of classical FDTD and Laguerre-SVD ROM has already been explored recently in the context of a subcell approach, but restricted to the 2D case [14, 15]. The method uses reduced-order modeling as a means to generate sub-

Correspondence to: D. De Zutter; email: daniel.dezutter@intec.rug.ac.be.

DOI 10.1002/mmce.20067

Published online 10 January 2005 in Wiley InterScience (www.interscience.wiley.com).

cell equations for a portion of space only. This subcell model can then be incorporated in an overall FDTD algorithm [16, 17]. This technique has proven to be able to simulate large 2D structures with a repetitive geometry [18], for example, photonic crystals [19]. However, the 3D combination of FDTD and ROM makes a subcell approach [9] computationally unattractive because of the much-too-large dimensions of input and output vectors of the subcell model. In 2D, a 20×20 subgridding domain requires about $20 \times 4 = 80$ independent input and output variables, whereas a comparably complex 3D example would demand about $6 \times 20^2 = 2400$ independent variables. Too much input/output variables substantially reduce the efficiency of the subcell technique. A more convenient way of simulating 3D examples, is treating the simulation examples as simple single input/single output systems (SISO), with a current source as the input and a voltage recorder as the output. This is exactly what will be presented in this contribution.

The rationale behind the choice of the Laguerre-SVD (LSVD) technique for model-order reduction is related to its frequency properties. It has been shown that with LSVD a broadband robust model-order reduction is possible, due to the excellent properties of the LSVD model-order reduction algorithm. In [8], a numerically very challenging benchmark [20] was reduced, clearly supporting the above statement. The advantageous properties of the Laguerre-SVD algorithm with respect to reciprocity were discussed in [21] and compared with balanced realisations in [22]. The combination of the Yee-cell-based discretisation and LSVD allows us to circumvent the small time-step problems of classical FDTD. The final output of the algorithm is a matrix function of the Laplace variable s describing the impedance relationship between the input current and the output voltage.

This article is further organised as follows. Section II discusses the formulation of the problem in terms of a state-space description. In section III, Krylov-based ROM methods are briefly introduced, followed by a general, as yet unpublished, proof of the preservation of the moment matching when expanding the transfer function as a function of σ, whereby σ is a particular Möbius transform of the original Laplace variable s. In section IV, some important issues on the iterative calculation of the Krylov matrix are discussed. Section V presents three numerical examples of increasing complexity, showing that the new method proposed here is capable of handling both low and high frequencies, even for structures that are several wavelengths long. Specific attention is devoted to the comparison of the simulation results with classical FDTD solver and with results obtained using the Padé via Lanczos (PVL) reduced-order modeling algorithm [20]. However, we restrict ourselves to lossless structures. Future research will focus on including the skin effect.

II. STATE SPACE DESCRIPTION

In order to obtain a state-space description, the spatial derivatives of the 3D Maxwell's equations for a charge-free region are discretised, with the fields sampled at the coordinates $(i\Delta, j\Delta, k\Delta)$, subsequently written as (i, j, k). The E- and H-fields are intertwined according to the standard Yee-type [2] arrangement of fields. This automatically implements the two divergence equations and implies 2nd-order accuracy in the space discretisation, whereas the time derivative remains untouched. The equations for the time derivatives, for example, of the x-components of the electric and magnetic fields for a source free region are given by

$$\mu_0\mu_{r,ijk}\dot{H}^x_{ijk} = \Delta^{-1}E^y_{ijk+(1/2)} - \Delta^{-1}E^y_{ijk-(1/2)} + \Delta^{-1}E^z_{ij-(1/2)k} - \Delta^{-1}E^z_{ij+(1/2)k},$$

$$\varepsilon_{r,ijk}\varepsilon_0\dot{E}^x_{ijk} = \Delta^{-1}H^z_{ij+(1/2)k} - \Delta^{-1}H^z_{ij-(1/2)k} + \Delta^{-1}H^y_{ijk-(1/2)} - \Delta^{-1}H^y_{ijk+(1/2)} - \sigma_{ijk}E^x_{ijk}. \quad (1)$$

The equations for the y and z directions are cyclic permutations hereof. The simulation domain Ω is a region of dimensions $(N_x\Delta, N_y\Delta, N_z\Delta)$. The boundary surfaces of this region are terminated with 1st-order Mur [23] absorbing boundary conditions (ABCs). Although general excitation conditions can be taken into account, we will from now on assume that the region Ω will be excited by soft electrical-current density sources J_s [2] defined along a source line AB between two conductors, as depicted in Figure 1. The imposed current is $u_I = J_s\Delta^2$. On this same figure, the recording of electric fields along the line CD between two other conductors, is also depicted. These fields determine the recorded voltage, defined by $y_V = \Sigma_r E_r\Delta$, with the index r running over the recorder-line electric fields ($r = 3$ in Fig. 1). We now write the field equations (1), together with the current excitation and the recording of the voltage, in terms of a state-space description as follows:

$$\boldsymbol{C}\dot{\boldsymbol{x}} = -\boldsymbol{G}\boldsymbol{x} + \boldsymbol{B}u_I,$$

$$y_V = \boldsymbol{L}^T\boldsymbol{x}. \quad (2)$$

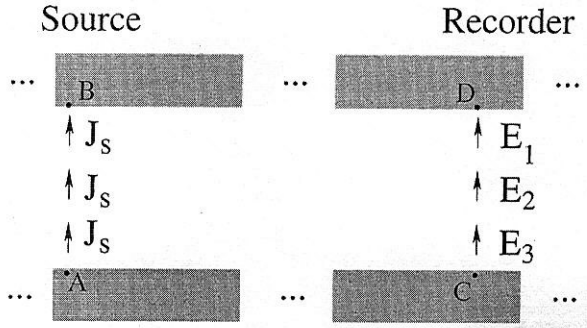

Figure 1. Construction of a current-density source input and a voltage recorder along two lines, each positioned between two conductors.

The vector x contains all the E-field and H-field variables, the scalar u_I is the imposed current and the scalar y_V is the recorded voltage. The C-matrix contains the permittivities of the media and the G-matrix stores the conductivities and the topological connectivity information. The C- and G-matrices are large but sparse. Their dimensions are $N_{sys} \times N_{sys}$ with $N_{sys} = \dim(x)$ being the system dimension. $\boldsymbol{B}$ and $\boldsymbol{L}$ are selection matrices. $\boldsymbol{B}$ represents the distribution of the source current u_I over the source geometry. $\boldsymbol{L}$ sums (discretised integration) the electric fields, leading to the output voltage y_V. The application of the 1st-order Mur ABC also leads to a 1st-order time-domain differential equation, which can easily be incorporated into the state-space description of eq. (2). We Laplace transform the system and, because iterative methods will be used in a following step, we further rescale the system according to $\tilde{s} = (\Delta/c_0)s$ and $\tilde{H} = R_0 H$, with R_0 being the free space impedance and c_0 the light speed in vacuum. For notational simplicity, we drop the tildes on all variables and matrices. The system is consequently rewritten as

$$\begin{aligned} s\boldsymbol{C}x &= -\boldsymbol{G}x + \boldsymbol{B}u_I, \\ y_V &= \boldsymbol{L}^T x. \end{aligned} \tag{3}$$

The transfer function $H(s) = \boldsymbol{L}^T(s\boldsymbol{C} + \boldsymbol{G})^{-1}\boldsymbol{B}$ is then a scalar impedance function of s with $y_V(s)/u_I(s) = H(s)$. With a proper choice of sources and recorders, any component of the $\boldsymbol{Z}$-matrix of a system can be modeled.

The main challenge that remains is that of reducing the very large number of internal variables N_{sys} to a much smaller amount while preserving the response of the system, including guaranteed passivity, and this at least in the frequency region of interest. The reduced system that we are looking for is similar to eq. (3), that is,

$$\begin{aligned} s\boldsymbol{C}_R z &= -\boldsymbol{G}_R z + \boldsymbol{B}_R u_I, \\ y_V &= \boldsymbol{L}_R^T z, \end{aligned} \tag{4}$$

where $\boldsymbol{C}_R$, $\boldsymbol{G}_R$, $\boldsymbol{L}_R$, and $\boldsymbol{B}_R$ are the reduced counterparts of $\boldsymbol{C}$, $\boldsymbol{G}$, $\boldsymbol{L}$, and $\boldsymbol{B}$, respectively, and z is the internal-variable vector of the reduced system, with $q = \dim(z) \ll \dim(x)$ and with $H_R = \boldsymbol{L}_R^T(s\boldsymbol{C}_R + \boldsymbol{G}_R)^{-1}\boldsymbol{B}_R$ the transfer function of the reduced system.

III. LOW- AND HIGH-FREQUENCY ROBUST MODEL ORDER REDUCTION

The next step in the simulation is to select a ROM method which guarantees a correct representation of the low-frequency response. To this end, we will first discuss the frequency properties of a certain class of Krylov subspace methods. These methods are related by a Möbius transform, because their transfer function $H(s)$ can be written [24] as a function of the Möbius transformed variable $\sigma = \mathcal{M}(s) = -[(b - sd)/(a - sc)]$ with $ad - bc \neq 0$ and $a, b, c, d \in \mathbb{R}$. Substituting for σ, $H(\sigma)$ becomes:

$$H(\sigma) = (c\sigma + d)\boldsymbol{L}^T(\boldsymbol{I} - \sigma\boldsymbol{A})^{-1}\boldsymbol{R}, \tag{5}$$

where $\boldsymbol{A} = -(d\boldsymbol{G} + b\boldsymbol{C})^{-1}(c\boldsymbol{G} + a\boldsymbol{C})$ and $\boldsymbol{R} = (d\boldsymbol{G} + b\boldsymbol{C})^{-1}\boldsymbol{B}$. We now Taylor expand [24, 25] $(\boldsymbol{I} - \sigma\boldsymbol{A})^{-1}$ in eq. (5), which is allowed, provided the spectral radius (the norm of the largest eigenvalue) $\rho(\sigma\boldsymbol{A})$ of the matrix $\sigma\boldsymbol{A}$ is smaller than unity:

$$H(\sigma) = (c\sigma + d)\sum_{i=0}^{\infty} \boldsymbol{L}^T\boldsymbol{A}^i\boldsymbol{R}\sigma^i = (c\sigma + d)\sum_{i=0}^{\infty} M_i\sigma^i. \tag{6}$$

It is clear that the choice of $\sigma = \mathcal{M}(s)$ will determine the convergence radius of the Taylor expansion and thus determine the performance of the chosen ROM method as a function of frequency. The transfer function $H_R(s)$ of the reduced system can similarly be written as

$$H_R(\sigma) = (c\sigma + d)\sum_{i=0}^{\infty} (M_R)_i\sigma^i. \tag{7}$$

The matching of M_i with $(M_R)_i$ for the first q moments, that is, $i = 1, \ldots, q - 1$, was first proven [6] for $\mathcal{M}(s) = s$, but will be generalised here for any Möbius transform. The matching remains possible if

we can find an orthogonal matrix V of size $N_{sys} \times N_{Rsys}$ whose columns form a basis for the Krylov space $\mathcal{K}(A, R, q) = \text{colspan}\boldsymbol{K} = \text{colspan}([\boldsymbol{R}, \boldsymbol{AR}, \boldsymbol{A^2R}, \ldots \boldsymbol{A^{q-1}R}])$. $N_{Rsys} = q$ is the dimension of the reduced system. The matrices of the reduced system then are $\boldsymbol{C_R} = \boldsymbol{V^TCV}$, $\boldsymbol{G_R} = \boldsymbol{V^TGV}$, $\boldsymbol{B_R} = \boldsymbol{V^TB}$, and $\boldsymbol{L_R} = \boldsymbol{V^TL}$. The moments of the reduced system are given by

$$(\boldsymbol{M_R})_i = \boldsymbol{L_R^T}[-(b\boldsymbol{C_R} + d\boldsymbol{G_R})^{-1}(a\boldsymbol{C_R} + c\boldsymbol{G_R})]^i\boldsymbol{R_R}$$
$$= \boldsymbol{L^T}[-\boldsymbol{V}(b\boldsymbol{C_R} + d\boldsymbol{G_R})^{-1}\boldsymbol{V^T}(a\boldsymbol{C} + c\boldsymbol{G})]^i\boldsymbol{VR_R}. \quad (8)$$

For $i = 0, 1, \ldots, q-1$, these moments need to be equal to the corresponding moments of the original system:

$$\boldsymbol{M_i} = \boldsymbol{L^TA^iR} = \boldsymbol{L^T}[-(b\boldsymbol{C} + d\boldsymbol{G})^{-1}(a\boldsymbol{C} + c\boldsymbol{G})]^i\boldsymbol{R}. \quad (9)$$

As $\boldsymbol{V}$ is a basis for the right Krylov subspace $\mathcal{K}$, each column of the defining Krylov matrix $\boldsymbol{K}$ is a linear combination of the basis vectors: $\boldsymbol{A^iR} = \boldsymbol{VE_i}$. Here, the values of E_i are a set of basis vectors of the subspace. For the first moment $i = 0$, this means that $(b\boldsymbol{C} + d\boldsymbol{G})^{-1}\boldsymbol{B} = \boldsymbol{VE_0}$. Multiplying this expression with $\boldsymbol{V}(b\boldsymbol{C_R} + d\boldsymbol{G_R})^{-1}\boldsymbol{V^T}(b\boldsymbol{C} + d\boldsymbol{G})$, we obtain

$$\text{l.h.s.} = \boldsymbol{V}(b\boldsymbol{C_R} + d\boldsymbol{G_R})^{-1}\boldsymbol{V^TB} = \boldsymbol{VR_R},$$
$$\text{r.h.s.} = \boldsymbol{V}(b\boldsymbol{C_R} + d\boldsymbol{G_R})^{-1}(b\boldsymbol{C_R} + d\boldsymbol{G_R})\boldsymbol{E_0}$$
$$= \boldsymbol{VE_0} = \boldsymbol{R}, \quad (10)$$

which proves $\boldsymbol{VR_R} = \boldsymbol{R}$ and shows the matching of the first moment $\boldsymbol{M_0} = (\boldsymbol{M_R})_0$. Then, we need to prove by induction that for $i > 0$, $[-\boldsymbol{V}(b\boldsymbol{C_R} + d\boldsymbol{G_R})^{-1}\boldsymbol{V^T}(a\boldsymbol{C} + c\boldsymbol{G})]^i\boldsymbol{R} = \boldsymbol{A^iR}$. We multiply this expression by $\boldsymbol{V}(b\boldsymbol{C_R} + d\boldsymbol{G_R})^{-1}\boldsymbol{V^T}(b\boldsymbol{C} + d\boldsymbol{G})\boldsymbol{A}$, which results in

$$\text{l.h.s.} = \boldsymbol{V}(b\boldsymbol{C_R} + d\boldsymbol{G_R})^{-1}\boldsymbol{V^T}(b\boldsymbol{C} + d\boldsymbol{G})(-1)(b\boldsymbol{C} + d\boldsymbol{G})^{-1}(a\boldsymbol{C} + c\boldsymbol{G})[-\boldsymbol{V}(b\boldsymbol{C_R} + d\boldsymbol{G_R})^{-1}\boldsymbol{V^T}(a\boldsymbol{C} + c\boldsymbol{G})]^i = -\boldsymbol{V}(b\boldsymbol{C_R} + d\boldsymbol{G_R})^{-1}\boldsymbol{V^T}(a\boldsymbol{C} + c\boldsymbol{G})[-\boldsymbol{V}(b\boldsymbol{C_R} + d\boldsymbol{G_R})^{-1}\boldsymbol{V^T}(a\boldsymbol{C} + c\boldsymbol{G})]^i = [-\boldsymbol{V}(b\boldsymbol{C_R} + d\boldsymbol{G_R})^{-1}\boldsymbol{V^T}(a\boldsymbol{C} + c\boldsymbol{G})]^{i+1},$$

$$\text{r.h.s.} = \boldsymbol{V}(b\boldsymbol{C_R} + d\boldsymbol{G_R})^{-1}\boldsymbol{V^T}(b\boldsymbol{C} + d\boldsymbol{G})\boldsymbol{AA^iR} = \boldsymbol{V}(b\boldsymbol{C_R} + d\boldsymbol{G_R})^{-1}\boldsymbol{V^T}(b\boldsymbol{C} + d\boldsymbol{G})\boldsymbol{VE_{i+1}} = \boldsymbol{VE_{i+1}} = \boldsymbol{A^{i+1}}, \quad (11)$$

thus concluding the proof.

In the Padé via Lanczos (PVL) technique [20], a method where stability cannot always be guaranteed, the choice for σ is $\sigma = s - s_0$. As a consequence, for the PVL method, the series of eq. (6) is only valid for expansion points $|s - s_0| < 1/\rho(A)$. Choosing $\sigma = s^{-1}$, as in [13], has the advantage that the matrices $\boldsymbol{A}$ and $\boldsymbol{R}$ are very easy to calculate for systems where C is diagonal, but the resultant expansion is only valid for $|s^{-1}| < 1/\rho(A)$, that is, for high frequencies. Because of the disadvantages of each of the above choices for σ, an in-between approach is adopted here, defined by $\sigma = \mathcal{M}(s) = [(s - \alpha)/(s + \alpha)]$. This particular choice for σ is the choice that leads to the Laguerre-SVD (LSVD) method. The mathematical and numerical properties of this method are discussed in [7]. The Möbius transform corresponding to the LSVD techniques is determined by $a = b = \alpha$, $c = -1$, $d = 1$ and thus the matrices defining the Krylov space $\mathcal{K}$ are given by

$$\boldsymbol{A} = -(\alpha\boldsymbol{C} + \boldsymbol{G})^{-1}(\alpha\boldsymbol{C} - \boldsymbol{G}),$$
$$\boldsymbol{R} = (\alpha\boldsymbol{C} + \boldsymbol{G})^{-1}\boldsymbol{B}. \quad (12)$$

IV. CALCULATION OF THE LSVD MOMENTS WITH LSQR

From eq. (12), it can be seen that the construction of the Krylov space $\mathcal{K}$ involves several inversions of large, unsymmetrical, and sparse matrices. We have chosen to apply the LSQR [26] algorithm because it is an iterative inversion method designed for solving matrix systems with these particular properties. A number of other iterative inversion methods have been extensively tested, but none of them gave better results. BICG [27] showed to be about four times slower for most examples, and BICGSTAB [28] sometimes stopped. In the LSQR method, the first inversion involves calculating $\boldsymbol{R}$. Choosing $\boldsymbol{B}$ as a starting vector only speeds up the inversion with a negligible amount (about 1%). The calculation of the other moments $\boldsymbol{M_i}$ for $q > 0$ requires the same matrix inversion for a different right-hand side and can also be implemented iteratively. In typical cases, the matrices $(\alpha\boldsymbol{C} \pm \boldsymbol{G})$ are well conditioned, even for structures with several different dielectrics. Moreover, these matrices are very sparse due to the large dimension of the typical 3D simulations considered here: the number of nonzero entries per matrix row never exceeds six. As such, it can be expected (but not proven) that the inversion will converge quickly. The more than 50 examples that were run proved this expectation to

be real. Moreover, the number of iterations for the first two inversion was always about 25% less than for the third and next inversions. From then on, the number of iterations does not change significantly for subsequent inversions. The convergence of eq. (6) becomes accelerated [7] for well chosen σ, with the optimal choice $\alpha = 2\pi f_{\max}$ with $f_{\max}$ the bandwidth of the system. This is in accordance with the observation that the σ-domain expansion boils down to the multiplication of a sum of allpass filters with a bandpass filter with cut-off frequency $f_{\max}$. The LSVD algorithm is summarised below.

LSVD-LSQR ROM Algorithm

1. Write down the voltage/current system of state-space equations, as defined in eq. (3);
2. Solve $(\boldsymbol{G} + \alpha \boldsymbol{C})\boldsymbol{R}_0 = \boldsymbol{B}$ with LSQR;
3. For $k = 1, \ldots, q-1$ solve $(\boldsymbol{G} + \alpha \boldsymbol{C})\boldsymbol{R}_k = (\boldsymbol{G} - \alpha \boldsymbol{C})\boldsymbol{R}_{k-1}$ with LSQR;
4. Calculate $\boldsymbol{U}\boldsymbol{\Sigma}\boldsymbol{V}^T = SVD([\boldsymbol{R}_0 \boldsymbol{R}_1 \cdots \boldsymbol{R}_{q-1}])$;
5. Calculate the following:
$$\boldsymbol{C}_R = \boldsymbol{U}^T \boldsymbol{C} \boldsymbol{U},$$
$$\boldsymbol{G}_R = \boldsymbol{U}^T \boldsymbol{G} \boldsymbol{U},$$
$$\boldsymbol{B}_R = \boldsymbol{U}^T \boldsymbol{B},$$
$$\boldsymbol{L}_R = \boldsymbol{U}^T \boldsymbol{L};$$
6. thus, the reduced order model is $H_R(s) = \boldsymbol{L}_R^T (s\boldsymbol{C}_R + \tilde{\boldsymbol{G}}_R)^{-1} \boldsymbol{B}_R$ with s being the rescaled Laplace variable associated with eq. (3).

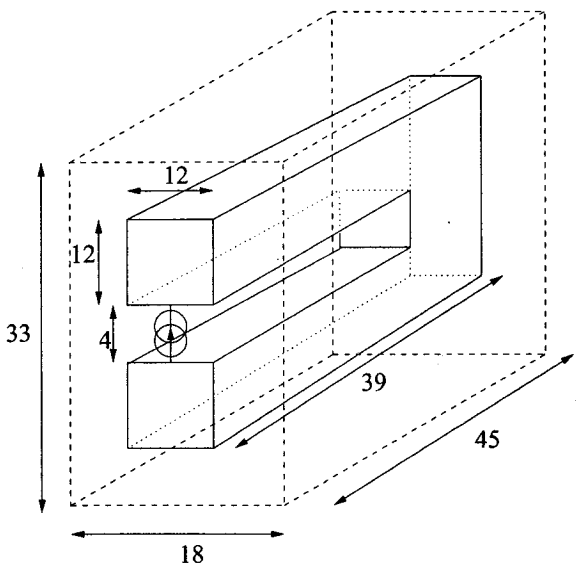

Figure 2. A u-shaped PEC interconnect structure.

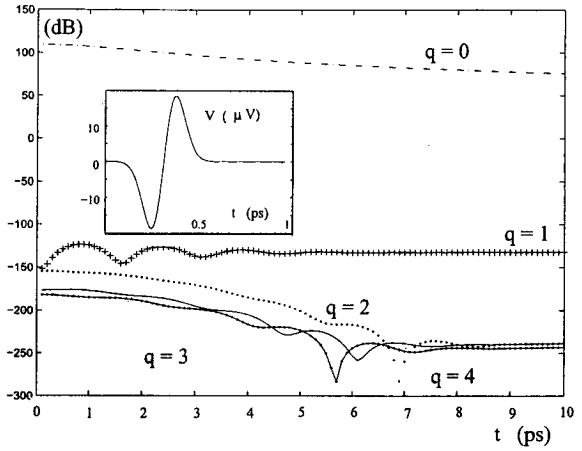

Figure 3. Comparison of the responses of standard FDTD and time-stepped LSVD for a u-shaped perfectly conducting interconnect.

V. NUMERICAL EXAMPLES

A. Simple U-Shaped Structure: Comparison with Standard FDTD

The simplest structure we will consider here is a u-shaped perfectly conducting interconnect. In Figure 2, this u-shaped structure is depicted together with its excitation. The simulation box with six ABC planes is also shown. The complete simulation volume measures $33 \times 18 \times 45 = 26730$ elementary cubic cells of side $\Delta = 1$ mm. The excitation is a current density source defined as $J_s = \sin(2\pi f_0 t) e^{-(t-t_0)^2/\tau^2} A/m^2$ with $t_0 = 30$ ps and $\tau = 1$ ps. The voltage is also recorded at the input location, so as to extract the input impedance. The central frequency $f_0 = 5$ GHz.

Comparison with direct FDTD results provides an indication on whether or not the inversions in the LSVD algorithm suffer numerical problems. Also, possible problems with the implementation of the boundary conditions can be detected. None of these problems were found, which is clearly shown in Figure 3. We have calculated the input voltage as a function of time. Figure 3 shows the absolute value of the relative difference in dB between the output voltage directly obtained with FDTD (V^F), as shown in the insert of Figure 3, and the value obtained with the approach presented in this paper (V^S). The time stepping of the ROM model can easily be performed by discretising the time variable of the reduced system and by executing the leapfrog algorithm with the internal variables vector z as the to be updated quantity. The time step is chosen according to the Courant criterium. The five curves of Figure 3 correspond to an increasing amount (up to five) of matching mo-

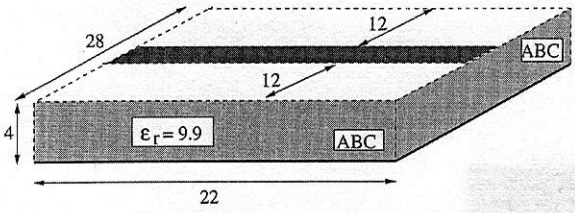

Figure 4. A transmission-line example which extends at four sides into the ABC planes.

ments M_i. Already from the second moment on (corresponding to the curve labeled $q = 1$) the agreement is excellent. The result may look promising, but we must not forget that the modeled structure is simple and small, and does not contain dielectrics nor losses.

B. A Typical Microstripline

To further check whether the applied ROM method preserves the performance of the 1st-order Mur ABCs, the obvious example to consider is a microstrip line. The actual structure we modeled is depicted in Figure 4. The PEC ground plane and the dielectric terminate into four ABC planes and the PEC strip itself terminates into two ABC planes, thus simulating an infinitely long microstrip on an infinite substrate. The elementary space step is 30.48 μm. All dimensions are shown in terms of this elementary space step. To be able to clearly assess the effect of the contrast at the dielectric-air interface, we have selected an ε_r value of 9.9. The structure is excited with a current source at the middle of the microstrip line. The resultant voltage is also recorded at the same location.

The effect of the ABC planes is that the equivalent circuit corresponding to the modeled structure is that of two parallel half-infinite transmission lines. Hence, the input impedance should be half that of the characteristic impedance of the microstrip line. The result shown in Figure 5 is practically independent of frequency, at least up to 20 GHz. The real part of the

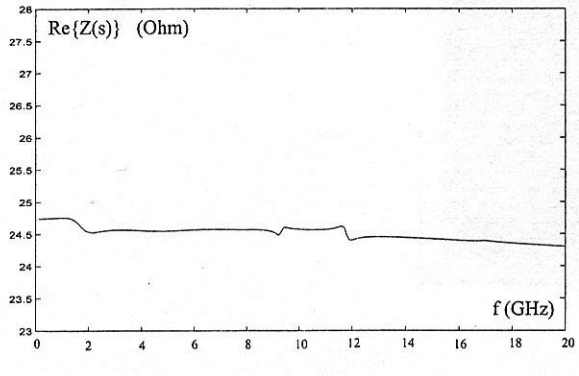

Figure 5. Input impedance of the microstrip line in Fig. 4.

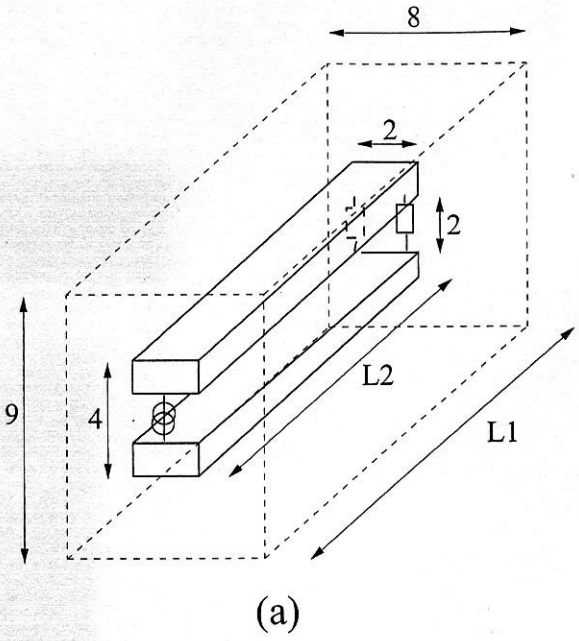

Figure 6. Parallel-plate transmission-line example.

impedance calculated by the LSVD algorithm was bounded by $24.3\Omega < Z(s) < 24.8\Omega$. Wheeler's closed-form formula yielded $Z_c/2 = 24.58\Omega$, while the 2D full-wave simulator (ADS from Agilent) yielded $Z_c/2 = 24.52\Omega$ at 1 GHz, $Z_c/2 = 24.51\Omega$ at 10 GHz, and $Z_c/2 = 24.51\Omega$ at 20 GHz. The reduced system has a dimension of $q = 75$ and no more than 900 LSQR iterations were needed to calculate each moment.

C. A Terminated Parallel-Plate Transmission Line

Next we consider a series of parallel-plate transmission line examples, one of which is depicted in Figure 6. The line is terminated symmetrically by a parallel network of two lumped resistances of $240\pi\Omega$ each. In this way, the DC input impedance of the line should be the free-space wave impedance. The elementary space step is 1 mm. The transmission line length is $L2 = 30$ mm. The length of the simulation box is $L1 = 35$ mm, with cross-sectional dimensions of 8 mm by 9 mm. The transversal dimensions of the parallel plates are 2×1 mm. The simulation volume counts $8 \times 35 \times 9 = 2520$ elementary cells and, hence, about six times more fields variables being 14295 field variables exactly. The transmission line is embedded in free space and the conductors are perfectly conducting.

The real part of the simulated input impedance is depicted in Figure 7 as a function of frequency and up

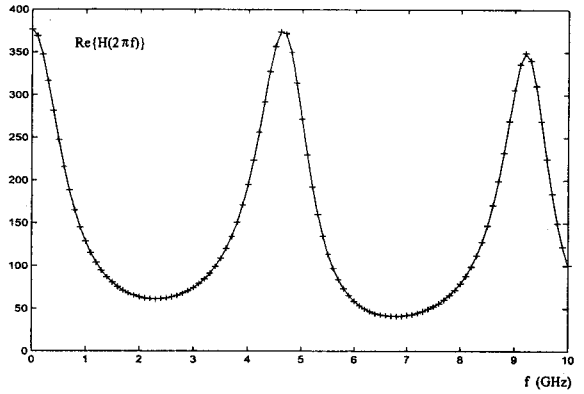

Figure 7. Comparison of the transfer function of the example in Fig. 6 with $L2 = 30$ mm and $L1 = 35$ mm obtained with LSVD [$q = 22$, full line] and with PVL [$q = 25$, crosses (+)].

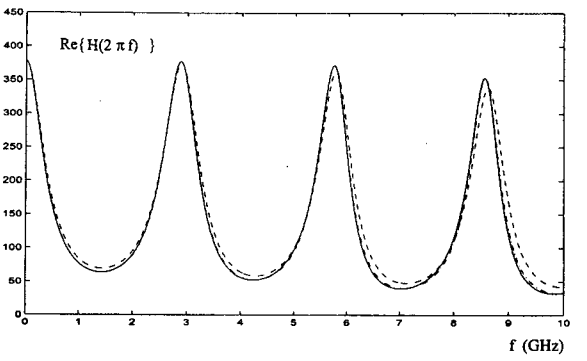

Figure 9. The transfer function of the example of Fig. 6 with $L2 = 50$ mm and $L1 = 55$ mm, obtained with LSVD ($q = 25$, full line, grid step = 1 mm), FDTD (dashed line, grid step = 0.5 mm), and FDTD (dashed-dotted line, grid step = 1 mm).

to 10 GHz, together with the result for a reduction of the state-space description using the PVL method [20]. The reduced systems have dimensions of $q = 22$ for the LSVD reduction and $q = 25$ for the PVL reduction. PVL matches $2q = 50$ moments whereas LSVD only needs $q = 22$ moments. The correspondence between both results is very good over the entire range. The number of LSQR iterations per inversion in the LSVD algorithm roughly remained constant and was on the order of 240. The LSVD reduction converges faster than PVL. This can be seen in Figure 8, which shows the real part of the transfer functions for reduced systems matching 20, 22, and 24 moments, respectively, as indicated in the figure. This difference in performance between LSVD and PVL will be further examined below.

If we take a very similar example, with the length of the transmission line extended to $L2 = 50$ mm and extending the simulation box to $L1 = 55$ mm, we obtain the following. The simulation box then counts $8 \times 55 \times 9 = 3960$ elementary cells, amounting to 24551 field variables.

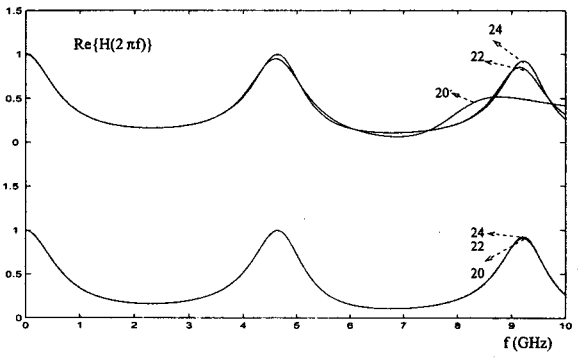

Figure 8. Reduced system response for the example of Fig. 6 with $L2 = 50$ mm and $L1 = 55$ mm for $2q = 20$, 22, and 24 moments matched with PVL (top) and $q = 20$, 22, and 24 moments matched with LSVD (bottom).

The real part of the transfer function for a reduction of $q = 25$ with LSVD is depicted in Figure 9, together with the simulation results of a standard FDTD simulation on an identical grid with space step $\Delta = 1$ mm. In the FDTD case, the frequency-domain transfer function was obtained by using the Fourier transforms of the current source and voltage time-domain signals. A third simulation result, also shown in the same figure, represents the real part of the transfer function obtained with standard FDTD, but on a grid which has a discretisation step $\Delta = 0.5$ mm. The results obtained with LSVD and FDTD on the 1-mm grid coincide almost completely. The FDTD results on a 0.5-mm grid differs slightly, the difference becoming more pronounced at higher frequencies, as can be expected. When we would simply model the parallel-plate transmission line as a 2D transmission line, the transfer function should vary between the load impedance $Z_L = 120\pi$ and $Z_c^2/Z_L = 56.5$, with $Z_c = 146\Omega$ the characteristic impedance of the 2D parallel-plate transmission line. In reality, important frequency-dependent 3D effects will come into play—in particular, at the beginning and the end of the line.

Again comparing the performance of the LSVD technique with that of the PVL technique, we see in Figure 10 that even for $q = 178$, PVL still has not reached convergence. The LSVD reduction needed about 250 iterations for each moment. The simulations for a transmission line of length 40 mm confirmed that PVL ultimately reaches convergence, but only for a much larger Krylov space than the one needed by LSVD. For the three different line lengths

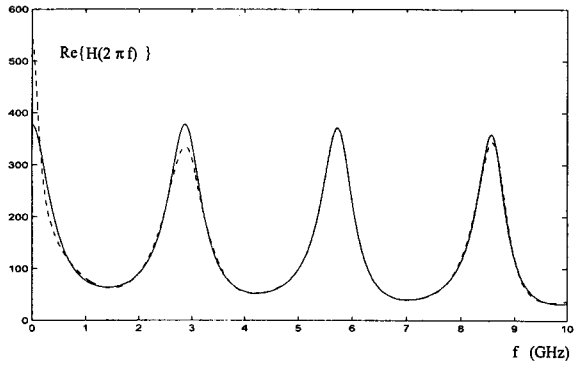

Figure 10. Comparison between LSVD (full line) and PVL (dashed line) for the example in Fig. 6 with $L2 = 50$ mm and $L1 = 55$ mm.

that we considered (30, 40, and 50 mm), the difference in the number of iterations needed for each moment matching when using the PVL method or the LSVD method was insignificant. As a consequence, the calculation times for systems with equal numbers of matched moments for both methods is almost equal. The 50-mm example needs 220, 233, 224, and 214 iterations for the calculations of the four first respective Krylov vectors ($0 \leq q < 5$). For $21 < q < 25$, the number of needed iterations is 179 for each of the three corresponding Krylov vectors. The construction of the Krylov matrix of size 24551×25 lasted 63.03 s. An additional 12.33 s were needed for the orthogonalizations with SVD of the Krylov spaces of size $9 < q < 25$ and the calculations of the respective transfer functions. The amount of memory needed is 95 MB. If the simulations are run with an embedding dielectric with $\varepsilon_r > 0$, the number of necessary LSQR iterations per moment increases, but not drastically. For the 50-mm example, an 8% increase for $\varepsilon_r = 3$ was observed, rising to about 30% for $\varepsilon_r = 10$.

The convergence of the LSQR method also depends on the grid step. However, as a consequence of the rescaling, typical problems converge well. In situations where the geometries require a finer meshing than required by the frequency content of the exciting signal (that is, typically $\lambda/20$), steps 2 and 3 of the LSVD-LSQR algorithm (13) will converge worse. However, this problem can be circumvented by choosing parameter α in eq. (13) to be much larger than the "optimal choice" of $2\pi f_{\max}$ put forward in [7]. This restores convergence at the cost of obtaining a larger Krylov space. The example of the 50-mm transmission line, calculated with $\alpha = 30 \times 2\pi f_{\max}$ converged at $q = 80$ instead of at $q = 25$ for $\alpha = 2\pi f_{\max}$ with $f_{\max} = 10$ GHz.

VI. CONCLUSIONS

In this article, we have introduced the combination of a Yee-cell-based discretisation of Maxwell's equations and a model-order reduction technique (LSVD) based on the expansion of the Laplace-domain transfer function in Laguerre polynomials. We have also proven the preservation of moment matching under a general Möbius transform of the Laplace variable s, of which LSVD is a special case. The final result of the approach presented in this article is a ready-to-use impedance function of frequency. The presented method proves to be very robust and guarantees the correct behavior at both low-frequency and high-frequency parts of the spectrum. The examples show that the LSVD technique outperforms the often-used PVL technique. For systems that are not too complex, the reduction factor (that is, the ratio of the original number of internal variables and the number of internal variables of the reduced system) is on the order of 10^3. Future efforts will be directed towards the inclusion of losses, a correct modeling of the high frequency skin effect, and an increase in the efficiency of the method in order to cope with very large state spaces.

ACKNOWLEDGMENT

The research activities leading to this contribution were supported by the Fifth Framework Programme of the European Community under contract no. IST-2001-34058 CODESTAR.

REFERENCES

1. A.E. Ruehli, Equivalent circuit models for three-dimensional multiconductor systems, IEEE Trans Microwave Theory Tech 22 (1974), 216–221.
2. A. Taflove, Computational electrodynamics: The finite-difference time-domain method, Artech House, Boston, 1995.
3. T. Weiland, Time-domain electromagnetical field computation with finite difference methods, Int J Num Modelling 9 (1996), 259–319.
4. www.cst.de/content/company/academic.aspx.
5. R.W. Freund, Krylov-subspace methods for reduced-order modeling in circuit simulation, J Comp Appl Math 123 (2000), 395–421.
6. A. Odabasioglu, M. Celik, and L.T. Pileggi, PRIMA: Passive reduced-order interconnect macromodeling algorithm, CAD Integ Circ Syst 17 (1998), 645–654.
7. L. Knockaert and D. De Zutter, Laguerre-SVD re-

duced-order modeling, IEEE Trans Microwave Theory Tech 48 (2000), 1469–1475.
8. L. Knockaert and D. De Zutter, Passive reduced order multiport modeling: the Padé–Laguerre, Krylov–Arnoldi SVD connection, AEÜ Int J Electron Commun 53 (1999), 254–260.
9. Ł. Kulas and M. Mrozowski, Reduced-order models of refined Yee's cells, IEEE Microwave Wireless Compon Lett 13 (2003), 164–166.
10. L. Zhao and A.C. Cangellaris, Reduced-order modeling of electromagnetic field interactions in unbounded domains truncated by perfectly matched layers, Microwave and Optical Tech Lett 17(1) (1998), 62–66.
11. R. Remis and P.M. van den Berg, A modified Lanczos algorithm for the computation of transient electromagnetic wavefields, IEEE Trans Microwave Theory Tech 45 (1997), 2139–2149.
12. A.C. Cangellaris, M. Celik, S. Pasha, and L. Zhao, Electromagnetic model order reduction for system-level modeling, IEEE Trans Microwave Theory Tech 47 (1999), 840–850.
13. A. Cangellaris and L. Zhao, Rapid FDTD simulation without time stepping, IEEE Microwave Guided Wave Lett 9 (1999), 4–6.
14. B. Denecker, F. Olyslager, L. Knockaert, and D. De Zutter, Automatic generation of subdomain models in 2-D FDTD using reduced order modeling, IEEE Microwave Guided Wave Lett 10 (2000), 301–303.
15. B. Denecker, D. De Zutter, L. Knockaert, and F. Olyslager, A higher-level algorithm for 2D electromagnetic modelling using an FDTD grid, Proc IEEE Antennas Propagat Soc Int Symp, Salt Lake City, UT, 2000.
16. B. Denecker, F. Olyslager, L. Knockaert, and D. De Zutter, Generation of FDTD subcell equations by means of reduced order modelling, IEEE Trans Antennas Propagat 51 (2003), 1806–1817.
17. B. Denecker, F. Olyslager, D. De Zutter, and L. Knockaert, 2D FDTD subgridding based on subdomain generation, URSI Int Symp Electromagn Theory (2001), 288–290.
18. B. Denecker, F. Olyslager, L. Knockaert, and D. De Zutter, Efficient FDTD analysis of very large finite photonic crystal structures, LEOS Benelux Photonic Crystal Workshop, Ghent, Brussels, 2002.
19. B. Denecker, F. Olyslager, D. De Zutter, L. Klinkenbusch, and L. Knockaert, Efficient analysis of photonic crystal structures using a novel FDTD-technique, IEEE Antennas Propagat Symp 2002, San Antonio, pp. 344–347.
20. P. Feldmann and R.W. Freund, Efficient linear circuit analysis by Padé approximation via the Lanczos process, IEEE Trans Computer-Aided Design 14 (1995), 639–649.
21. L. Knockaert and B. Denecker, Explicit reciprocity and reduced order modeling, 2001 URSI Int Symp Electromagn Theory, 2001, Boston, pp. 497–499.
22. L. Knockaert, B. Denecker, and D. De Zutter, Explicitly reciprocal reduced order modeling: Laguerre-SVD versus balanced realizations, IEEE Antennas Propagat Symp Dig 2 (2002), 556–558.
23. G. Mur, Absorbing boundary conditions for the finite-difference approximation of the time-domain electromagnetic field equations, IEEE Trans Electromagn Compat 23 (1981), 377–382.
24. B. Denecker, The subdomain FDTD method, Ph.D. thesis, Ghent University, 2002–2003.
25. D.L. Boley, Krylov space methods on state-space control model, Circuits Syst Signal Process 13 (1994), 733–758.
26. C. Paige and M.A. Saunders, LSQR: An algorithm for sparse linear equations and sparse least squares, ACM Trans Mathem Software 8 (1982), 43–71.
27. R.M. Barrett, M. Berry, T.F. Chan, J. Demmel, J.M. Donato, J. Dongarra, V. Eijkhout, R. Pozo, C. Romine, and H. van der Vorst, Templates for the solution of linear systems: Building blocks for iterative methods, SIAM (1994).
28. H.A. van der Vorst, A fast and smoothly converging variant of bi-cg for the solution of nonsymmetric linear systems, SIAM J Sci Stat Comput 13 (1992), 631–644.

BIOGRAPHIES

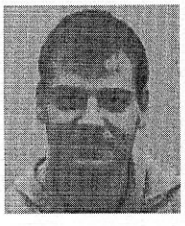

Gunther Lippens was born in Kortrijk, Belgium on April 12, 1974. He received his B.Sc. degree in electrical engineering in 1997 and his M.Sc. degree in physics engineering in 2000, both from Ghent University, Belgium. His research focuses on high-frequency interconnect modelling for packaging, on-chip interconnect and reduced-order modelling techniques. He is currently working towards a Ph.D. degree in the Electromagnetics Group of the Department of Information Technology of Ghent University, Belgium.

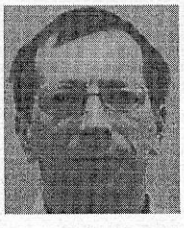

Daniël De Zutter was born in 1953. He received his M.Sc. degree in electrical engineering from Ghent University in 1976. From 1976 to 1984, he was a research and teaching assistant at the same university. In 1981 he obtained a Ph.D. degree and in 1984 he completed a thesis leading to a degree equivalent to the French Aggrégation or the German Habilitation. From 1984 to 1996, he was with the National Fund for Scientific Research of Belgium. He is now a full professor of electromag-

netics at the Department ofInformation Technology (Ghent University). Most of his earlier scientific work dealt with the electrodynamics of moving media. His research now focusses on all aspects of circuit and electromagnetic modelling of high-speed and high-frequency interconnections and packaging, electromagnetic compatibility (EMC), and numerical solutions of Maxwell's equations. As author or co-author, he has contributed to more than 130 international journal papers and 140 papers in conference proceedings. In 1993 he published a book titled "Electromagnetic and Circuit Modelling of Multiconductor Transmission Lines" (with N. Faché and F. Olyslager) in the Oxford Engineering Science Series. He received the 1990 Montefiore Prize of the University of Liège and the 1995 IEEE Microwave Prize Award (with F. Olyslager and K. Blomme) from the IEEE Microwave Theory and Techniques Society for best publication in the field of microwaves for the year 1993. In 1999 he received the Transactions Prize Paper Award from the IEEE EMC Society. In 2000 he was elected to the grade of Fellow of the IEEE.

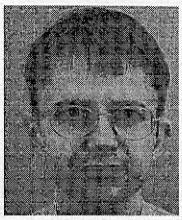

Frank Olyslager was born in 1966. He received his degree in electrical engineering in 1989 and his Ph.D. degree in 1993, both from Ghent University, Belgium. At present he is a Full Professor in electromagnetics at Ghent University. His research concerns different aspects of theoretical and numerical electromagnetics. He is Assistant Secretary General of URSI and was Associate Editor of *Radio Science.* He has authored or coauthored about 200 papers in journals and proceedings. He coauthored one book, "Electromagnetic and Circuit Modelling of Multiconductor Transmission Lines," and authored another book, "Electromagnetic Waveguides and Transmission Lines," both published by Oxford University Press. In 1994 he became Laureate of the Royal Academy of Sciences, Literature, and Fine Arts of Belgium. He received the 1995 IEEE Microwave Prize for the best paper published in the 1993 *IEEE Transactions on Microwave Theory and Techniques* and the 2000 Best Transactions Paper award for the best paper published in the 1999 *IEEE Transactions on Electromagnetic Compatibility.* In 2002 he received the Issac Koga Gold Medal at the URSI General Assembly.

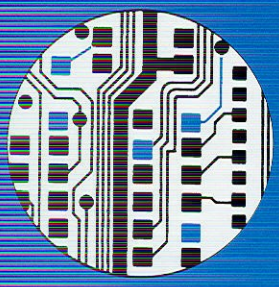

INTERNATIONAL JOURNAL OF

RF and Microwave Computer-Aided Engineering

VOLUME 15/NUMBER 2 MARCH 2005

WILEY Publishers Since 1807

Volume 15, Number 2 was mailed the week of March 14, 2005.

ISSN: 1096-4290